ACS OMEGA

Open Access

http://pubs.acs.org/journal/acsodf

Article

Size-Related Pathway Flux Analysis of Ultrasmall Iron Oxide Nanoparticles in Macrophage Cell RAW264.7 for Safety Evaluation

Jiaqing Guo,[§] Shixin Xu,[§] Usman Majeed, Jianming Ye, Huaxin Zhang, Weiming Xue, and Yane Luo*

Cite This: *ACS Omega* 2024, 9, 3480−3490

Read Online

ACCESS | Metrics & More | Article Recommendations

ABSTRACT: The endocytosis, intracellular transport, and exocytosis of different-sized nanoparticles were reported to greatly affect their efficacy and biosafety. The quantitation of endocytosis and exocytosis as well as subcellular distribution of nanoparticles might be an effective approach based on transport pathway flux analysis. Thus, the key parameters that could present the effects of three different-sized ultrasmall iron oxide nanoparticles (USIONPs) were systematically investigated in RAW264.7 cells. The endocytosis and exocytosis of USIONPs were related to their sizes; 15.4 nm of S2 could be quickly and more internalized and excreted in comparison to S1 (7.8 nm) and S3 (30.7 nm). In RAW264.7 cells, USIONPs were observed in endosomes, lysosomes, the Golgi apparatus, and autophagosomes *via* a transmission electron microscope. Based on flux analysis of intracellular transport pathways of USIONPs, it was found that 43% of S1, 40% of S2, and 44% of S3 were individually transported extracellularly through the Golgi apparatus-involved middle-fast pathway, while 24% of S1, 23% of S2, and 26% of S3 were transported through the fast recycling endosomal pathway, and the residues were transported through the slower speed lysosomal pathway. USIONPs might be transported *via* size-related endocytosis and exocytosis pathways. The pathway flux could be calculated on the basis of disturbance analysis of special transporters as well as their coding genes. Because there were rate differences among these transport pathways, this pathway flux could anticipate the intracellular remaining time and distribution of different-sized nanoparticles, the function exertion, and side effects of nanomaterials. The size of the nanomaterials could be optimized for improving functions and safety.

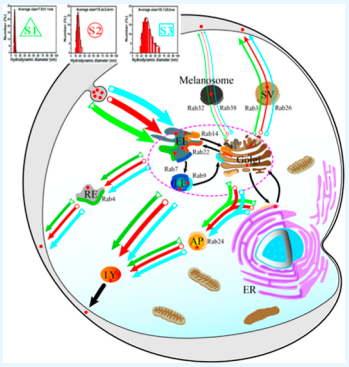

INTRODUCTION

Nanotechnology has been applied and developed in all aspects, especially biotechnology and biomedicine.[1,2] Among a wide variety of nanomaterials, iron oxide nanoparticles (IONPs) have been allowed by the U.S. Food and Drug Administration to be utilized in biomedicine owing to the excellent physicochemical properties and bioavailability, such as unique magnetic response, low toxicity, and side effects, easily being coupled with antibody or receptor ligands, *etc.*[3−5] Compared with the most commonly used gold magnetic nanoparticles, IONPs are bioactive, they can activate and cause macrophages to attack and even selectively kill cancer cells *via* increasing intracellular reactive oxygen species.[6−8] Currently, IONPs have been commercialized for the treatment of iron-deficient anemia (*e.g.*, Venofer commercialized by American Regent) and cancer treatment (*e.g.*, NanoTherm sold by MagForce).[9] Besides, IONPs have been gradually developed into nanoantibacterial agents, a smart release system for special nutrition or drugs, a magnetic separating system for cells, and a detecting system for pathogenic bacteria.[10,11]

At present, the size of commercial iron oxide diagnostic and therapeutic agents is mainly 20−300 nm. It has been proved that IONPs smaller than 20 nm are ideal contrasts and carriers, especially the ultrasmall magnetic IONPs less than 5 nm are expected to be developed into a new type of highly sensitive and nontoxic T1 contrast agent for early diagnosis of cancer.[12−15] However, with the further reduction of the size of nanoparticles, the dynamic behavior and biological effects of nanoparticles in and out of cells have changed greatly.[16] Ultrasmall IONPs (USIONPs) may pass through intestinal barrier, blood−brain barrier, and placental barrier through passive transport, and their distribution *in vivo* is unpredictable, which leads to the safety evaluation being more complicated.[17]

It has been found that USIONPs is mainly eliminated by phagocytosis of macrophages *in vivo* within 24−72 h.[18,19] The physicochemical properties of the nanomaterial themselves have been reported to affect the elimination mechanisms and results of macrophages, that is, chemical compositions, size, morphology and surface modification.[20−22] Consequently, there are many unclear and doubtable cognitions about the fate of IONPs after being phagocytized. For example, the subcellular distribution, intracellular transport and metabolism,

Received: September 15, 2023
Revised: December 20, 2023
Accepted: December 25, 2023
Published: January 10, 2024

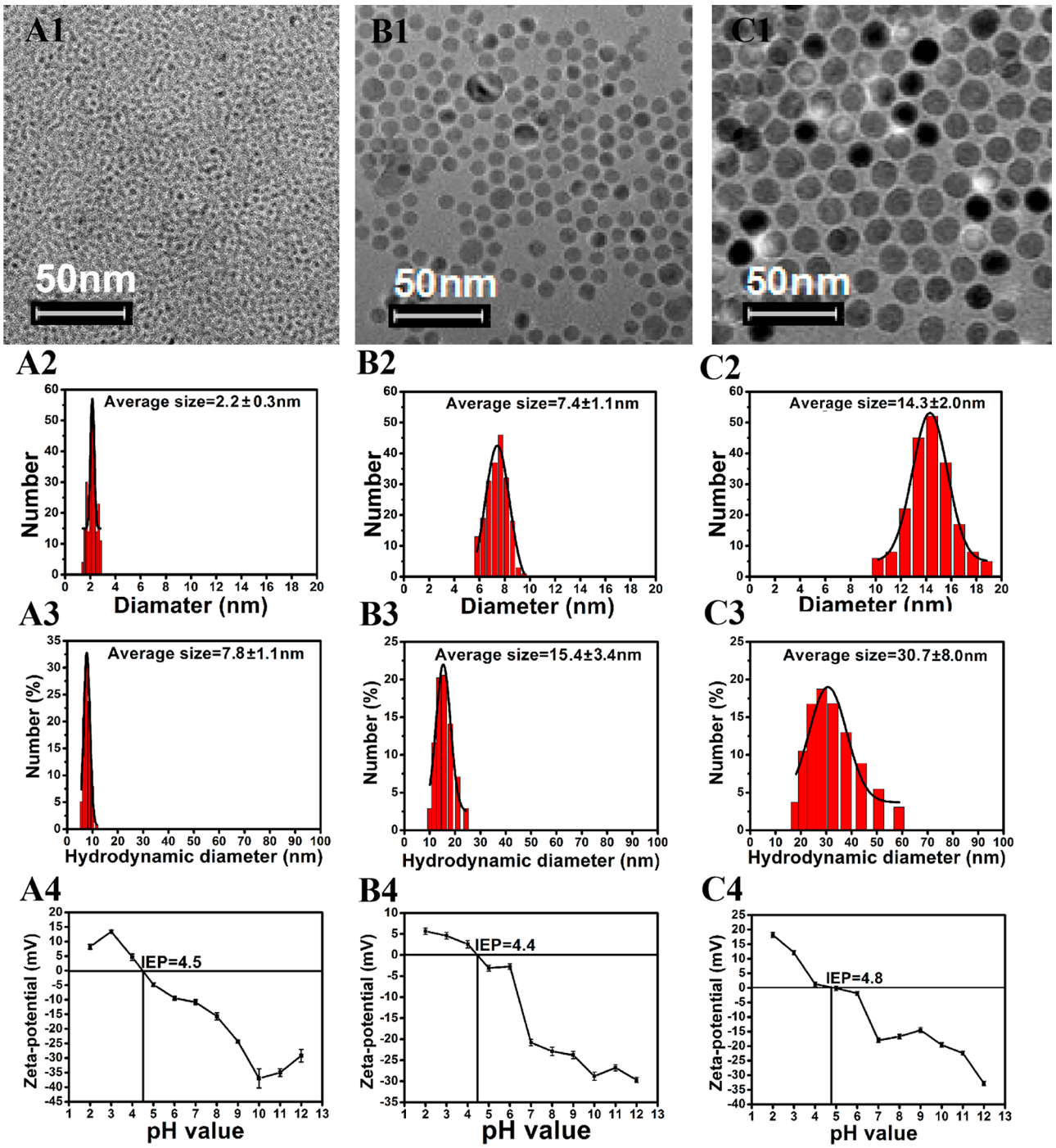

Figure 1. Appearance, TEM size statistics, hydration diameter, and zeta potential of IONPs. Panels (A1−A4) present TEM size, size in the oil phase, hydration diameter, and zeta potential of S1, respectively. Panels (B1−B4) show TEM size, size in the oil phase, hydration diameter, and zeta potential of S2, respectively. Panels (C1−C4) exhibit TEM size, size in the oil phase, hydration diameter, and zeta potential of S3, respectively.

and exocytosis of USIONPs are still unclear, but these obscure questions have been reported to determine the efficacy and safety of large-sized IONPs *in vitro* and *in vivo*.[23−25] With the development of precision medicine, the dynamically quantitative study of the intracellular distribution of IONPs has become inevitable and ignorable. Unfortunately, the analysis of intracellular transport pathways and their flux are rarely reported, which seriously limits the optimal design, function exertion, and application of IONPs. Therefore, it is urgent to quantify the subcellular distribution and intracellular transport of IONPs.

It is well-known that macrophages are the key components of the immune system, they patrol in most tissues *in vivo* and are always ready to phagocytize invasive pathogens or damage and repair damaged tissues.[26−28] It is also found that the transport efficiency of cancer nanodrugs can be improved to 600% by attracting macrophages into tumor blood vessels.[29] Therefore, RAW264.7 macrophages were chosen as the model cells in this study. Also, three different-sized IONPs were prepared to investigate the size effects on the dynamically intracellular distribution and exocytosis.[17] On the base of quantitative PCR analysis of transport protein, specific protein

https://doi.org/10.1021/acsomega.3c07081
ACS Omega 2024, 9, 3480−3490

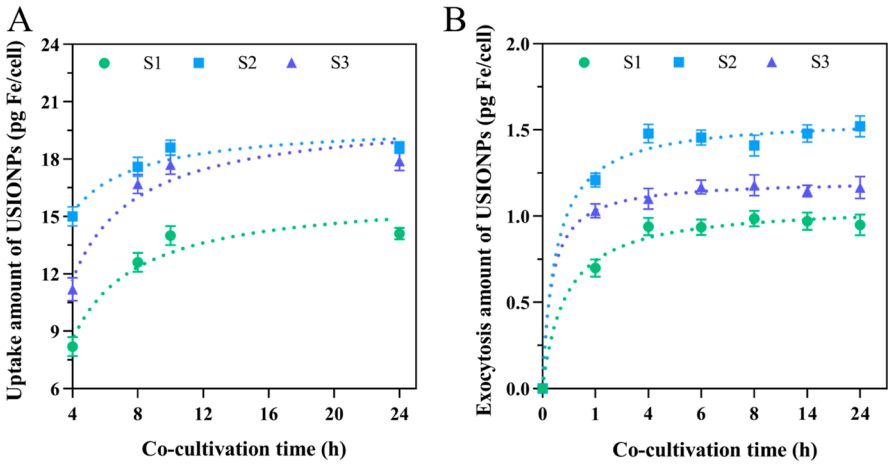

Figure 2. Dynamic uptake and exocytosis profile of USIONPs by RAW264.7 cells. Panels (A,B), respectively, describe the endocytosis and exocytosis kinetics of three different-sized USIONPs. The average particle hydrated sizes of three samples (S1, S2, and S3) were 7.8, 15.4, and 30.7 nm, respectively.

inhibitor interference, and siRNA technology, the endocytic and exocytose kinetics as well as transport pathways were established so as to clarify and calculate the subcellular distribution and intracellular transport of USIONPs. This research will beneficial to the optimization of design, targeting delivery, and controllable release of nanoparticles.[30] In particular, more effective and novel intelligent nano diagnostic and therapeutic agents will be designed, and these "nano missiles" *in vitro* and *in vivo* will become controllable on the basis of the true cognition of molecule mechanisms of the transport and metabolism.

MATERIALS AND METHODS

Chemicals and Materials. FeOOH, oleic acid (AR), octadecene (99.5%), *N*-hexane (AR), ethanol (99.5%), phosphorus oxychloride (AR), polyethylene glycol (molecular weight 2000), tetrahydrofuran, and so forth. All reagents are analytically pure. USIONPs measuring 7.8, 15.4, and 30.7 nm were prepared as previously reported.[31]

Cell Line and Culture. Macrophage cell RAW264.7 is derived from the cell bank of the Chinese Academy of Sciences, subcultured in our laboratory, and stored in liquid nitrogen. RAW264.7 cells were grown in RPMI-1640 medium supplemented with 10% FBS and 1% penicillin streptomycin solution in a humidified atmosphere of 5% CO_2 at 37 °C. Cells in the logarithmic growth phase were chosen for further study.[32]

Uptake Kinetics of USIONPs. USIONP solution was added into cells in the logarithmic growth phase with a set concentration of 40 μg/mL of Fe. RAW264.7 cells and USIONPs were cocultured for 4, 8, 10, and 24 h. After washing with PBS three times to remove USIONPs out of cells, the cells were collected, acidified, and digested to release iron and then intracellular iron was measured by ICP-MS (NexION, PE). Meanwhile, cell samples at each time point were counted *via* a fluorescence microscope (Ti2-A, Nikon). All experiments were done in triplicates.

Exocytosis Kinetics of USIONPs. RAW264.7 cells and USIONPs were cocultured for 10 h after washing with PBS three times to remove extracellular USIONPs. Then, fresh medium without nanoparticles was added for continued culture. RAW264.7 cells and fresh medium were cocultured for 1, 4, 6, 8, 14, and 24 h. Culture medium was collected, and extracellular iron was measured by ICP-MS (NexION, PE); meanwhile, the cell number was detected as mentioned above.

Imaging Analysis by Transmission Electron Microscopy. After being cocultured with USIONPs for 10 h, cells were continuously cultured in fresh medium without USIONPs for 1, 6, and 24 h (these special time points were selected in view of exocytosis kinetics of USIONPs), respectively. TEM was used to analyze the subcellular localization of nanoparticles at different time points to estimate the possible exocytosis pathways of USIONPs.

Real-Time Fluorescent Quantitative PCR Analysis of Rab Proteins. After being cocultured with USIONPs for 10 h, cells were continuously cultured in fresh medium without USIONPs for 1 h. Then, cells were harvested to extract RNA with a RNAprep Pure Cell kit (TaKaRa) in accordance with the manufacturer's instructions. Then, reverse transcription reactions with SYBR Premix Ex *Taq*II (TaKaRa) were immediately performed. qPCRs were carried out in 96-well plates in the CFX96 real-time PCR detection system (Bio-Rad Laboratories, USA). Also, the relative mRNA expression levels were estimated using the $2^{-\Delta\Delta CT}$ method.[33]

Disturbance Analysis. According to the manufacturer's transfection protocol, transfection of the cells with Si-RNA was performed using the Lipofectamine RNAiMAX reagent (Invitrogen; Thermo Fisher Scientific Inc.). After Si-RNA transfection by Exo1, fresh medium was replaced after coculture with USIONPs, and the inhibition degree of exocytosis was detected in the equilibrium period of exocytosis at the sixth hour. The miRNA expression level was detected by the qPCRs mentioned above.

Statistical Analysis. Results are shown as a mean ± standard deviation (SD) unless otherwise indicated. All of the data were evaluated using SPSS Statistics 21.0 (IBM, USA) and performed using GraphPad Prism 8 (GraphPad, USA). Statistical significance was calculated *via* one-way ANOVA with a Tukey s-b(k) test or Student's *t*-test. Differences were considered significant at $p < 0.05$.

RESULTS AND DISCUSSION

Characterization of Magnetic USIONPs. As shown in Figure 1A1−C1, the prepared oil-phase USIONPs were spherical with good monodispersity and uniform size distribution. The average particle sizes of three samples (S1,

https://doi.org/10.1021/acsomega.3c07081
ACS Omega 2024, 9, 3480−3490

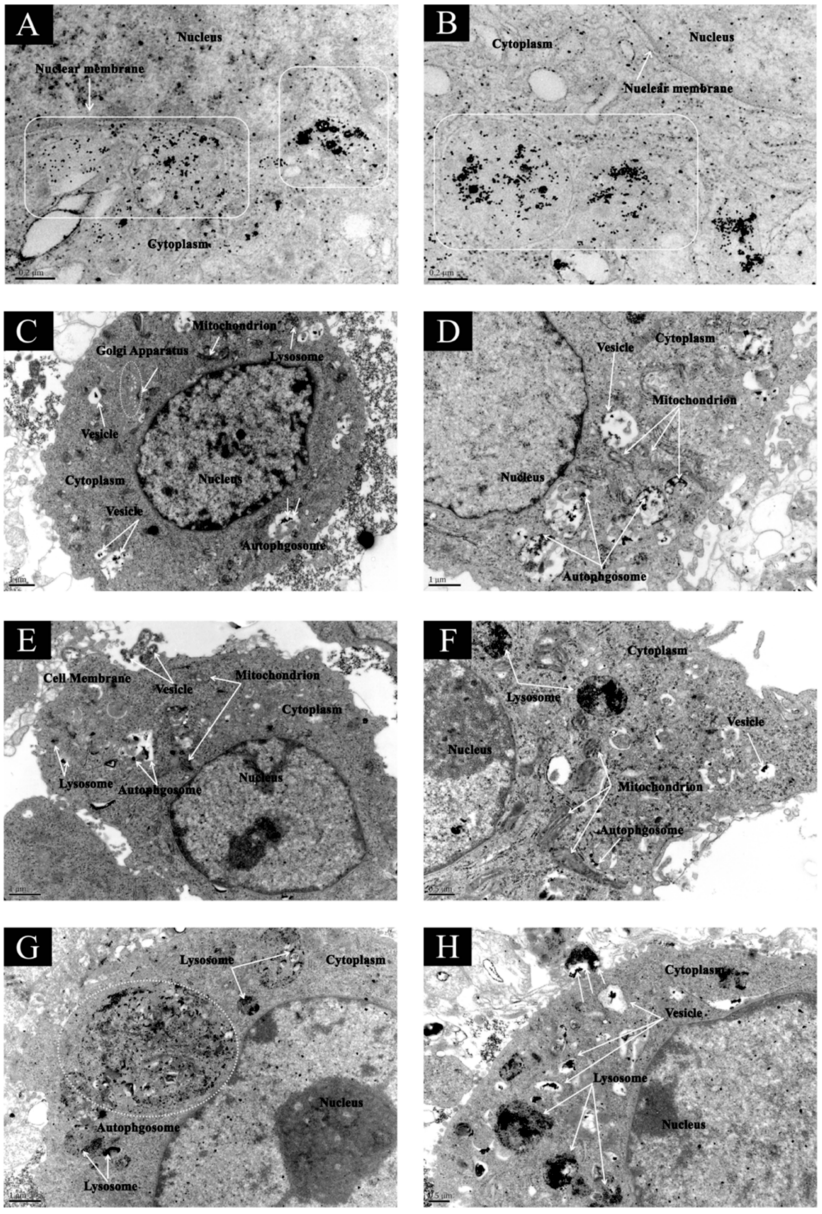

Figure 3. TEM images of USIONPs distributed in RAW264.7 cells. Picture (A) shows that small-sized S1 liked to be distributed around the nuclear region; picture (B) shows large-sized S2 might be difficult to enter into the nucleus; pictures (C,E,G), respectively, represent the distribution of USIONPs in RAW264.7 cells after the exocytosis process lasting for 1, 6, and 24 h; pictures (D,F,H), respectively, show the amplification of special zones in RAW264.7 cells after the exocytosis process lasting for 1, 6, and 24 h.

S2, and S3) were 2.2, 7.4, and 14.3 nm, respectively (Figure 1A2−C2).

With PEG surface modification, oleic acids on the surface of nanoparticles were replaced by PEG2000 molecules *via* a substitution reaction, thus a narrow size range of water-soluble USIONPs were produced. They were stable in the aqueous phase, and their hydrated diameters detected by dynamic light scattering were increased to 7.8 nm (S1), 15.4 nm (S2), and 30.7 nm (S3), respectively (Figure 1A3−C3). On the other hand, zeta potential reflected USIONP dispersion stability in water. As shown in Figure 1A4−C4, zeta values of aqueous S1, S2, and S3 under neutral conditions were −12.7, −20.8, and −18.0 mV, respectively, which suggest the stable dispersion of USIONPs in neutral medium. When the zeta potential was 0, the isoelectric points of S1, S2 and S3, were 4.5, 4.4, and 4.8, respectively, in an aqueous phase.

Endocytosis and Exocytosis Kinetics of Different-Sized USIONPs. Macrophages were cocultivated with three different-sized USIONPs with 40 μg Fe/mL dosages as previously reported.[34] With the prolongation of culture time, the total amount of nanoparticles entering into cells rapidly increased during the 0−10th hour and then became stable (Figure 2A). Therefore, 10 h of endocytosis was selected as the starting point to study exocytosis behaviors and rules. Meanwhile, the endocytosis of three different-sized USIONPs significantly appeared as a size effect. The maximum uptake amounts of S1, S2, and S3 were 14.1, 18.6, and 17.9 pg of Fe/cell, respectively. The least uptake of S1 was due to small nanoparticles having to overcome cytomembrane resistance when entering into cells, while S2 and S3 were easier to overcome cytomembrane resistance and permeate cytomembrane due to their larger size and mass. Thereby, the uptake

https://doi.org/10.1021/acsomega.3c07081
ACS Omega 2024, 9, 3480−3490

amounts of S2 and S3 were more than that of S1,[22,35−37] in agreement with previous research showing that the optimum cellular uptake of nanoparticles is achieved with sizes ranging from 10 to 50 nm.[38] García *et al.* found that 14 nm of gold nanoparticles have higher internalization efficiency than 5 nm in MDA.MB.231 cells.[39] Endocytosis is inhibited for <10 nm hard particles because of the high energy cost of membrane bending that is involved during cell−nanoparticle interactions and membrane wrapping around the nanoparticle.[37]

The exocytosis kinetics of nanoparticles coincided well with the single exponential model. The content of nanoparticles in the culture medium increased significantly during the first 4 h and then exocytosis of nanoparticles enhanced slowly after 4 h (Figure 2B), which coincided with the time needed to reach the maximum exocytosis in most reports.[40] The exocytosis rates reduced continuously due to the decreased driving force resulting from the concentration gradient difference between intracellular and extracellular USIONPs for nanoparticle efflux. Then, the dynamic equilibrium between endocytosis and exocytosis gradually approached; thus, the exocytosis number of nanoparticles did not further increase. The final exocytosis amounts of S1, S2, and S3 were 0.98, 1.48, and 1.18 pg of Fe/cell, respectively. In the coculture stage of nanoparticles and cells, the endocytosis of S1 and S3 was slightly lower than that of S2 and correspondingly a lower exocytosis of S1 and S3. A similar result was reported by Serda *et al.*, who found that 15 nm of USIONPs were easier to be excreted from macrophages than 30 nm of nanoparticles. A more plausible explanation was that small particle S2 had less receptor−ligand interactions compared to S3, leading to an easier release and faster removal.[22]

Additionally, according to TEM images (Figure 3A,B), S1 liked to be distributed around the nuclear region in comparison to S2 and S3, which made it difficult to discharge them out of cells.[41,42]

Subcellular Localization of Different-Sized USIONPs. As shown in Figure 3, TEM images of subcellular localization of different-sized USIONPs in RAW264.7 cells were obtained after cocultivated in fresh medium for 1, 6, and 24 h. At the first hour of exocytosis, it was observed that S2 was not only located in organelles such as endosomes, the Golgi apparatus, lysosomes, and mitochondria but also distributed in autophagosomes (Figure 3C,D). The endosomal vesicles existed near the cell membrane, which indirectly demonstrated that the endosomal vesicles played an important role in transporting nanoparticles across the cell membrane.

Furthermore, at the sixth hour of exocytosis, it was observed that USIONPs were excreted out of the cells *via* membrane fusion under the action of vesicle transport (Figure 3E). Besides, some USIONPs were still in the mitochondria. With the exocytosis process proceeding, the density of electron clouds in lysosomes increased, and the black color further deepened (Figure 3F), which indicates the increase of USIONPs in lysosomes. These USIONPs might be further transformed into secondary lysosomes to degrade.[43] At the 24th hour of exocytosis, the numbers of USIONPs in cells were decreased, while autophagosomes were gradually increased, and USIONPs in lysosomes seemed to be partially degraded (Figure 3G). Vesicles near the cell membrane continued to discharge the overloaded USIONPs through membrane fusion (Figure 3H).

Summarily, USIONPs might be excreted *via* the Golgi apparatus or endosomal vesiculation near the membrane.[43] Additionally, USIONPs might also trigger autophagy to form autophagosomes for exocytosis or degradation.[44]

Analysis of Exocytosis Pathways of Different-Sized USIONPs Based on Genomics. Usually, the responding transporters were overexpressed under the stimulation of special cargoes. Thus, the intracellular transporters for USIONPs were quantitatively tested *via* real-time fluorescent quantitative PCR to clarify the main transport pathways constituted of essential transporters and their regulatory proteins. It is well-known that nanoparticles are mainly transported inside and out of cells through vesicles that are mediated by Rab proteins, and Rab proteins play an essential role in membrane transport systems in all eukaryotic cells.[45,46] The Rab proteins involving intracellular transport and efflux, from Rab3 to Rab38, were quantitatively detected. The key Rab proteins involving the intracellular transport network and efflux of different-sized USIONPs are shown in Figure 4. Due to the size effects of USIONPs, three main transport pathways mediated by Rab proteins were analyzed as follows.

Transport Pathway Involving Early Endosomes and/or Late Endosomes, Golgi, and Exocytosis. Based on the gene expression level of Rab proteins, it was found that S1 inhibited the expression of Rab22, while S2 and S3 promoted the

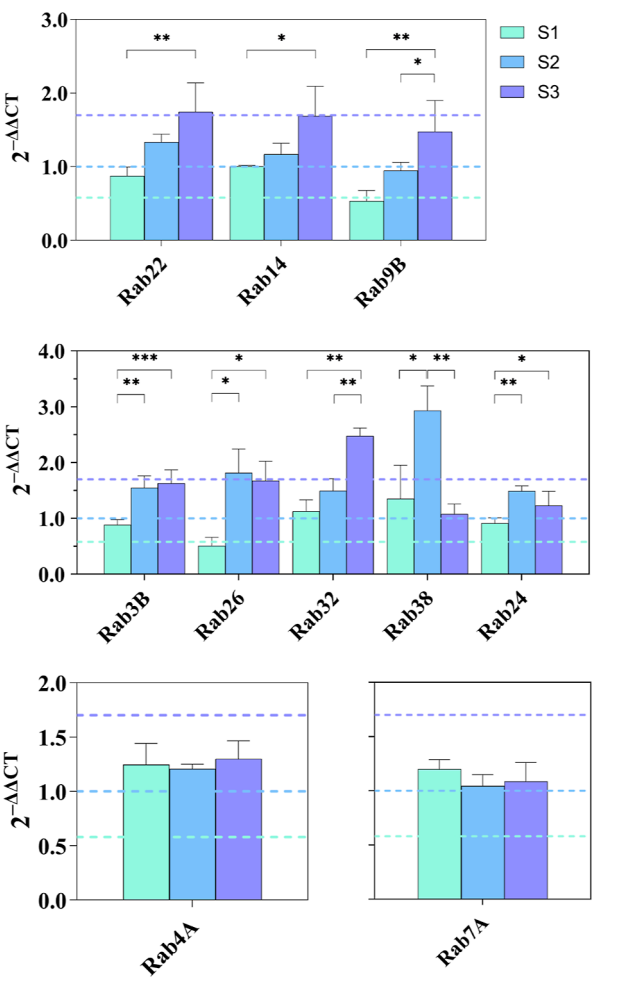

Figure 4. Quantitative analysis of key vesicle transporters (Rab proteins) during the process of exocytosis of USIONPs. Data are presented as mean ± standard deviation (n = 3). Statistical significance was calculated *via* one-way ANOVA with a Tukey s-b(k) test. P values: *P < 0.05, **P < 0.01, ***P < 0.001.

https://doi.org/10.1021/acsomega.3c07081
ACS Omega 2024, 9, 3480−3490

expression of Rab22 (Figure 4). After USIONPs entered into cells, they were first trapped into the early endosomes. The vesicular transport between the early endosome and the Golgi apparatus was bidirectionally regulated by Rab22.[47] Moreover, transport from early endosome to the Golgi apparatus was unidirectionally regulated by Rab14.[45,48] The expression levels of Rab22 and Rab14 responding for USIONPs from early endosome to the Golgi apparatus were enhanced in a decreasing order of S3, S2, and S1 (Figure 4).

Rab7, residing in late endosomes and mediating vesicular transport from early to late endosomes and/or lysosomes, was slightly stimulated by USIONPs without significant size influence, indicating little difference among the transport of these three different-sized nanoparticles from early to late endosomes. The transport of USIONPs from late endosomes to the Golgi apparatus was shunted by Rab9.[45,49] The size effect of USIONPs on Rab9 was similar to that of Rab22 and Rab14, *i.e.*, S3 stimulated the highest expression of Rab9 (Figure 4), which meant that large-sized nanoparticles were more easily transported from late endosomes to the Golgi apparatus.[50] However, S1 inhibited the expression of Rab9. With the increase of size of USIONPs, the expression of RAB9 increased, indicating that large-sized nanoparticles were more likely to select the branching pathway from the late endosomes to the Golgi apparatus.

After being repackaged by a Golgi apparatus, USIONPs were then secreted *via* secretory vesicles; this process involved transporter Rab3B and Rab26. S1 inhibited the expression of Rab3B, while S2 and S3 significantly promoted the expression of Rab3B. The changing trend of the gene expression of Rab26 along with the sizes of USIONPs was consistent with that of Rab3B, which also demonstrated the Golgi apparatus efflux *via* the secretory vesicle pathway mediated by Rab3 and rab26.[48,51] The expression of Rab3 and rab26 was inhibited by S1, indicating that the efflux of S1 from the *trans*-Golgi *via* the secretory vesicle pathway was lower than that of S2 and S3. However, there was no significant difference of the expression of Rab3 and Rab26 stimulated by S2 and S3.

Meanwhile, all three sizes of USIONPs promoted the expression of Rab32 and Rab38. Under the action of Rab32 and Rab38 proteins, the vesicles transporting USIONPs were transferred from the late endosomes to the trans-Golgi apparatus. These vesicles have further formed the melanosomes and then excreted out of cells.[50] Among them, the comprehensive expression levels of Rab32 and 38 stimulated by S2 were higher, while that of S1 was not significant. Rab32 and Rab38 were involved in the biogenesis of melanosomes and Rab32 also controlled mitochondrial fission.[45,47] S3 activated only the overexpression of Rab32 rather than Rab38, inferring that S3 may strengthen mitochondrial fission. Furthermore, the melanosome pathway for transporting S3 was similar to that of S1.

S2 promoted the expression of Rab24, while S1 inhibited the Rab24 expression. Rab24 mediated the formation of the preautophagosomal structure to engulf nanoparticles into the Golgi apparatus and endoplasmic reticulum, with formation of the autophagosomes.[45,52] The autophagosomes were subsequently targeted to the lysosomes, and finally, nanoparticles were discharged out of cells through cell membrane fusion. The expression of Rab24 stimulated by S2 was the highest, indicating that the discharge of S2 *via* the autophagosome pathway was greater than that of S1 and S3. Furthermore, S1 could not be excreted through this pathway. Interestingly, there seemed to be a complementary competition between the autophagosome pathway mediated by Rab24 and the pathway from late endosomes to lysosomes mediated by Rab7 (Figure 4). Because lysosomes and autophagosomes play similar roles in some way, the increase of the flux to lysosome pathway would indirectly lead to the decrease of autophagosome flux.[53]

Based on gene expression and TEM images, it could be speculated that the exocytosis of USIONPs usually occurred through the Golgi apparatus pathway.[47] First, under the regulation of Rab14 and Rab22, a part of nanoparticles located in the early endosome were directly transferred to the Golgi apparatus, and another were encapsulated by early endosomes to further develop into late endosomes and transported to the Golgi apparatus. Then, under the action of Rab3 and Rab26, the Golgi apparatus network formed typical secretory vesicles to excrete USIONPs out of cells, or melanosomes were formed by the trans-Golgi apparatus for further excretion. The gene expression levels of Rab proteins mediating the Golgi pathway were in the increasing order of S1, S2, and S3. Moreover, the expression of Rab proteins responding for the melanosome pathway and autophagosome pathway for S2 was significantly greater than that for S1 and S3, which further illustrated the diversity of intracellular transport and exocytosis pathways of S2. S1 in the Golgi apparatus rarely transported or degraded, leading to the accumulation around the nuclear region as shown in TEM images (Figure 3A).

Transport Pathway from Early Endosomes and Recycling Endosomes to Exocytosis. Three different-sized USIONPs promoted the expression of Rab4, *i.e.*, the shunting pathway from early endosomes to recycling endosomes was activated, which was also evidenced by TEM images. After entering into cells, USIONPs were preferentially trapped into early endosomes, then from early endosomes to recycling endosomes, and finally transported outside *via* recycling endosomes.[54] Notably, the expression levels of Rab4 had little difference after treatment with three different-sized USIONPs.

Transport Pathway from Early Endosomes and Late Endosomes to Lysosomes. As reported, there might be a complementary relationship between the lysosome pathway and Golgi pathway for transporting nanoparticles.[53] S1, S2, and S3 impacted a slight overexpression on Rab7, which implied that the USIONPs in early endosomes would be transformed into late endosomes. Moreover, Rab7A expression increased slightly by S1 compared to that by S2 and S3, indicating that there might be little difference among the pathway fluxes of three different-sized USIONPs from late endosomes to lysosomes. With the gradual decrease of pH value from early endosomes and late endosomes to exocytosis, USIONPs moved to lysosomes to be degraded or eliminated by cells.[21,55−57] The TEM images of cells treated by S2 further corroborated the existence of the lysosome pathway; lysosomes abundantly existed in cytoplasm and might degrade the overloaded nanoparticles.

Generally, in view of the expression levels of crucial transporters and mediators, S1 might be captured by early endosomes and then transported through the recycling endosome pathway mediated by Rab4 and the late endosome pathway mediated by Rab7, and there seemed an inhibition to the Golgi apparatus pathway as well as the autophagy pathway for degradation. S2 might be transported, excreted, and degraded *via* the Golgi apparatus pathway (including melanosome secretion and autophagosome degradation), recycling endosomal pathway, and lysosomal pathway. S3

https://doi.org/10.1021/acsomega.3c07081
ACS Omega 2024, 9, 3480−3490

showed a trend similar to that of S2. There was a size effect on the transport of nanoparticles, which was very important to optimize the size design of nanoparticles. For example, small-sized nanoparticles (similar to S1) could be designed to play functions after lysosomal degradation.[38] Contrastingly, the route of endosome−Golgi−endoplasmic reticulum (ER) was exploited as a safe trafficking pathway for nanodrug transportation, such as cholera toxin and some virus-mediated drug delivery systems.[58,59]

Flux Analysis of Transport Pathways of USIONPs. *Flux Analysis of the Golgi Apparatus-Involving Pathway.* According to the gene expression analysis of key Rab proteins that played an important role in exocytosis pathways, S2 and S3 were both transported *via* the pathways constructed by early endosomes or late endosomes, the Golgi apparatus, and exocytosis. It could be inferred that the Golgi apparatus involving-pathway was one of the main exocytosis pathways for differently sized USIONPs. It has been reported that 2-(4-fluorobenzoylamino)-benzoic acid methyl ester (Exo1) can induce the collapse of the Golgi apparatus and function as a chemical inhibitor of the exocytosis pathway.[48,51,60] After treatment by Exo1, the reduction percentages of exocytosis to S1, S2, and S3 were 15.77, 12.96, and 13.08%, respectively (Figure 5). The inhibitor Exo1 was to change the membrane structure of Golgi apparatus, such as typical secretory vesicles and melanosomes. Thus, the Golgi apparatus involving exocytosis pathways was perturbed, and finally, exocytosis amount was significantly decreased. Furthermore, siRNA interference against Rab26 mediating the secretory vesicle pathway was programed, and the exocytosis percentages of S1, S2, and S3 were individually reduced by 11.30, 10.34, and 8.82%, respectively. Based on the mass conservation principle, *i.e.*, the core principle of flux analysis, it could be calculated that the decline ratios of the melanosome pathway of S1, S2, and S3 were correspondingly 4.47, 2.62, and 4.26%.

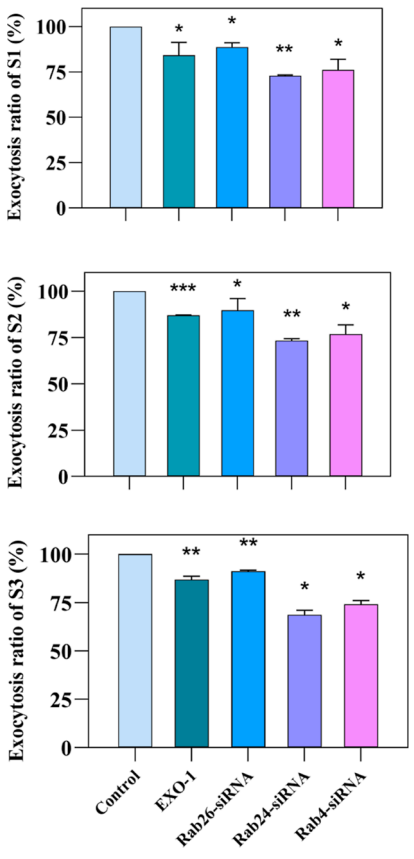

Figure 5. Inhibition degrees of different exocytosis pathways. Mean values ±standard deviation, $N = 3$. *$p < 0.05$, **$p < 0.01$ and ***$p < 0.001$ when compared with the control group (Student's *t*-test).

By siRNA interference against Rab24 protein relating to the autophagy pathway, the decreased percentages of exocytosis of S1, S2, and S3 were 27.10, 26.70, and 31.33%, respectively. These significant decreases in the efflux of nanoparticles indicated that excessive nanoparticles remaining in the Golgi apparatus and endoplasmic reticulum would be cleaned out through the autophagy pathway. According to the flux of the Golgi apparatus and autophagy pathway, the total fluxes relating to the Golgi apparatus for transporting S1, S2, and S3 were 42.87, 39.66, and 44.41%, respectively, being close to the reported 40% distribution of the pathway including the Golgi apparatus.[51] Compared to the other transport pathways, inhibition of the Golgi apparatus involving pathways would be the maximal in the vesicle transport network. Based on the multiple flux decline ratios, the actual exocytosis amount of three different-sized USIONPs through this pathway was ranked as S2 > S3 > S1.[41] Moreover, many organelles participated in the Golgi apparatus pathway, it was the most extended chain pathway, and the entire chain node also carried most of the overloaded nanoparticles.

Flux Analysis of the Recycling Endosome-Involving Pathway. By siRNA interference against Rab4 protein mediating the recycling endosome pathway, the decreased percentages of exocytosis of S1, S2, and S3 were 23.83, 23.15, and 25.80%, respectively (Figure 5).[54] The obvious decreases in the exocytosis amount also indirectly demonstrated that the recycling endosome pathway was one of the most dominant routes for discharging nanoparticles. It is reported that this pathway is also the fastest pathway among many exocytosis pathways, and it is expected to start within a few minutes after endocytosis.[30,61,62] As the total exocytosis amount, S2 was much higher than that of S3 and S1, and the actual exocytosis amounts of three different-sized USIONPs passing through this pathway were ranked as S2 > S3 > S1.

Flux Analysis of the Lysosome-Involving Pathway. From early endosomes to lysosomes, there was a branch pathway at the node of late endosomes, and this pathway flux could be calculated by disturbing another branch approach. As shown in Figure 6, the organelles including early endosomes, late endosomes and Golgi circled by a dashed elliptical line were viewed as a whole transfer station. Then, there were one influx pathway and five efflux pathways. The influx of USIONPs was set as 100% and the net accumulation at every transport organelle was presumed as zero, fluxes of the Golgi apparatus-involved pathway (secretory vesicle pathway, melanosome pathway, and autophagy pathway) and recycling endosome pathway were measured *via* disturbance tests, *i.e.*, these four pathway efflux ratios were known as above, the last pathway fluxes from late endosomes to lysosomes for S1, S2, and S3 could be calculated and were 33.30, 37.19, and 29.79%, respectively (Figure 6). This ratio coincided with the relevant report that approximately one-third of internalized FITC-nanoceria colocalized with lysosomes.[38] Moreover, S1 and S2 in the lysosome pathway were more than that of S3, in agreement with previous research showing that 4 to 22 nm sized gold nanoparticles were degraded *in vitro* by lysosomes in fibroblasts.[38]

https://doi.org/10.1021/acsomega.3c07081
ACS Omega 2024, 9, 3480−3490

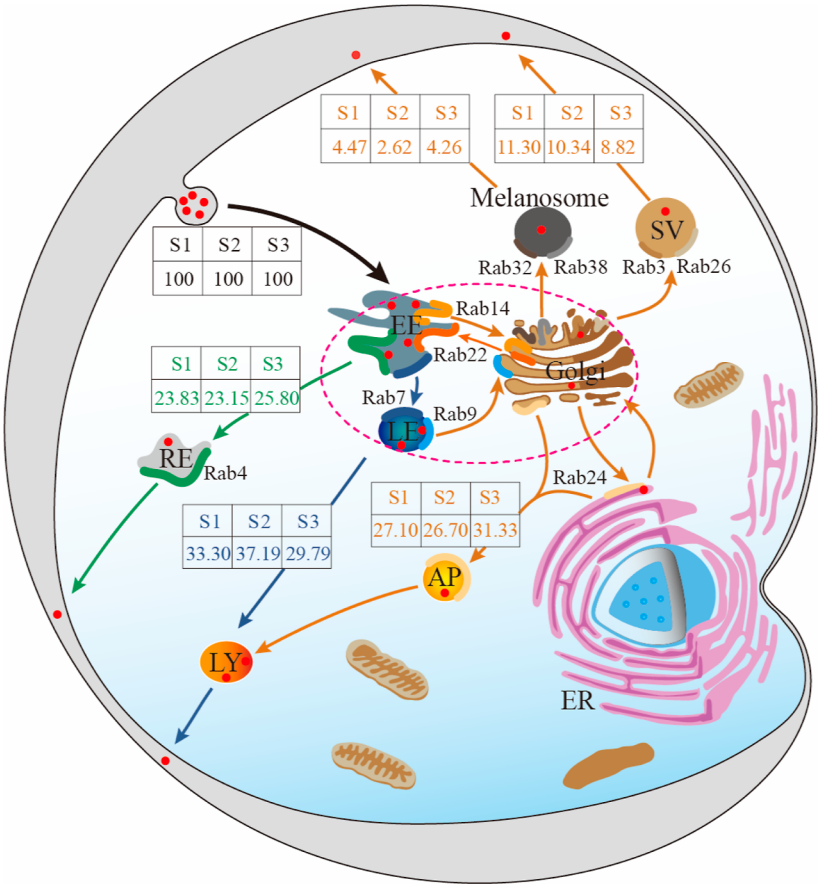

Figure 6. Flux distribution of intracellular transport pathways and exocytosis of different-sized USIONPs. Abbreviations: AP, autophagosome; EE, early endosome; ER, endoplasmic reticulum; LE, late endosome; LY, lysosome; RE recycling endosome; and SV, secretory vesicle.

Excessive USIONPs would cause cells to bear pressure for a short time, and they would first initiate the recycling endosome pathway to discharge them. Taking S2 as an example, the recycling endosome pathway probably shared about 23% of the total influx; ∼ 40% of USIONPs would flow to the Golgi apparatus with secreting 13% of USIONPs to outside of cells; 27% of USIONPs remained in the Golgi apparatus, and endoplasmic reticulum would be excreted and degraded through the autophagy pathway. Because so many organelles were involved in the Golgi apparatus pathway, this transport journey was complicated, thus the duration of USIONPs was the longest.[30] With time, USIONPs that could not be transported in time would slowly move into lysosomes coupling the maturation of early endosomes into late endosomes, finally degraded in lysosomes. In our study, about 37% of S2 might be degraded, which needed further research.

Generally, most USIONPs captured in early endosomes were of high mobility, whereas those in late endosomes and lysosomes were of low mobility. It would take about half an hour for nanoparticles from cells to enter lysosomes.[43] The majority of USIONPs were carried by this pathway in the early and middle stages, until the nanoparticles were transported to the transfer station, Golgi apparatus.[36,43,61] Since the total exocytosis amount of S2 was much higher than that of S3 and S1, the actual exocytosis amount of three different-sized USIONPs passing through this pathway was ranked as S2 > S3 > S1.

CONCLUSION

There is a size effect in endocytosis and exocytosis of three different-sized USIONPs. After endocytosis, USIONPs were located in organelles such as endosomes, Golgi apparatus, lysosomes and mitochondria, and autophagosomes. Also, these organelles could form the transport pathways for USIONPs, *i.e.*, the Golgi apparatus involving pathways—recycling endosomal pathway and lysosomal pathway. Based on disturbance analysis of special transporters as well as their coding genes, the recycling endosome pathway for transporting S2 probably shared about 23% of the total influx; ∼ 40% of S2 would flow to the Golgi apparatus secreting 13% of S2 to outside of cells; 27% of S2 remained in the Golgi apparatus and endoplasmic reticulum would be excreted and degraded through the autophagy pathway; and about 37% of S2 might escape and/or be degraded through the lysosomal pathway. The transport pathway fluxes of S1 and S3 also could be measured and calculated as S2. Since there were rate differences among these transport pathways, the size-related remaining time of nanomaterials could be anticipated, thus the function exertion and side effects of nanomaterials could be prejudged. Finally, size optimization could be realized and work, especially improving functions and safety of nanomaterials.

AUTHOR INFORMATION

Corresponding Author

Yane Luo − *College of Food Science and Technology, Northwest University, Xi'an 710069, China;* orcid.org/0000-0002-0273-1195; Email: luoyane@nwu.edu.cn

https://doi.org/10.1021/acsomega.3c07081
ACS Omega 2024, 9, 3480−3490

Authors

Jiaqing Guo − *School of Chemical Engineering, Northwest University, Xi'an 710069, China;* orcid.org/0000-0003-4841-2517

Shixin Xu − *School of Chemical Engineering, Northwest University, Xi'an 710069, China*

Usman Majeed − *College of Food Science and Technology, Northwest University, Xi'an 710069, China*

Jianming Ye − *College of Food Science and Technology, Northwest University, Xi'an 710069, China*

Huaxin Zhang − *School of Chemical Engineering, Northwest University, Xi'an 710069, China*

Weiming Xue − *School of Chemical Engineering, Northwest University, Xi'an 710069, China*

Complete contact information is available at: https://pubs.acs.org/10.1021/acsomega.3c07081

Author Contributions

[§]J.G. and S.X. contributed equally to this work.

Notes

The authors declare no competing financial interest.

■ ACKNOWLEDGMENTS

This work was financially supported by the National Key Research and Development Program of China (grant no. 2019YFC1606704) and Key Research and Development Program of Shaanxi Province (grant no. 2022NY-013).

■ ABBREVIATIONS

AP, autophagosome; EE, early endosome; ER, endoplasmic reticulum; LE, late endosome; LY, lysosome; RE, recycling endosome; SV, secretory vesicle

■ REFERENCES

(1) Zhu, W.; Wei, Z.; Han, C.; Weng, X. Nanomaterials as Promising Theranostic Tools in Nanomedicine and Their Applications in Clinical Disease Diagnosis and Treatment. *Nanomaterials-Basel* **2021**, *11* (12), 3346.

(2) Zhang, J.; Chang, D.; Yang, Y.; Zhang, X.; Tao, W.; Jiang, L.; Liang, X.; Tsai, H.; Huang, L.; Mei, L. Systematic investigation on the intracellular trafficking network of polymeric nanoparticles. *Nanoscale* **2017**, *9* (9), 3269−3282.

(3) Veiseh, O.; Gunn, J. W.; Kievit, F. M.; Sun, C.; Fang, C.; Lee, J. S.; Zhang, M. Inhibition of tumor-cell invasion with chlorotoxin-bound superparamagnetic nanoparticles. *Small* **2009**, *5* (2), 256−264.

(4) Mahmoudi, M.; Azadmanesh, K.; Shokrgozar, M. A.; Journeay, W. S.; Laurent, S. Effect of nanoparticles on the cell life cycle. *Chem. Rev.* **2011**, *111* (5), 3407−3432.

(5) Abo-zeid, Y.; Ismail, N. S. M.; McLean, G. R.; Hamdy, N. M. A molecular docking study repurposes FDA approved iron oxide nanoparticles to treat and control COVID-19 infection. *Eur. J. Pharm. Sci.* **2020**, *153*, 105465.

(6) Kim, S. E.; Zhang, L.; Ma, K.; Riegman, M.; Chen, F.; Ingold, I.; Conrad, M.; Turker, M. Z.; Gao, M. H.; Jiang, X. J.; Monette, S.; Pauliah, M.; Gonen, M.; Zanzonico, P.; Quinn, T.; Wiesner, U.; Bradbury, M. S.; Overholtzer, M. Ultrasmall nanoparticles induce ferroptosis in nutrient-deprived cancer cells and suppress tumour growth. *Nat. Nanotechnol.* **2016**, *11* (11), 977−985.

(7) Zanganeh, S.; Hutter, G.; Spitler, R.; Lenkov, O.; Mahmoudi, M.; Shaw, A.; Pajarinen, J. S.; Nejadnik, H.; Goodman, S.; Moseley, M.; Coussens, L. M.; Daldrup-Link, H. E. Iron oxide nanoparticles inhibit tumour growth by inducing pro-inflammatory macrophage polarization in tumour tissues. *Nat. Nanotechnol.* **2016**, *11* (11), 986−994.

(8) Tarangelo, A.; Dixon, S. J. Nanomedicine: An iron age for cancer therapy. *Nat. Nanotechnol.* **2016**, *11* (11), 921−922.

(9) Alphandéry, E. Iron oxide nanoparticles for therapeutic applications. *Drug Discov. Today* **2020**, *25* (1), 141−149.

(10) Krishna, V. D.; Wu, K.; Su, D.; Cheeran, M. C. J.; Wang, J. P.; Perez, A. Nanotechnology: Review of concepts and potential application of sensing platforms in food safety. *Food Microbiol.* **2018**, *75*, 47−54.

(11) Kaittanis, C.; Naser, S. A.; Perez, J. M. One-step, nanoparticle-mediated bacterial detection with magnetic relaxation. *Nano Lett.* **2007**, *7* (2), 380−383.

(12) Xu, L.; Wang, X.; Wang, R.; Liu, S.; Xu, M. Engineered Macrophages: A Safe-by-Design Approach for the Tumor Targeting Delivery of Sub-5 nm Gold Nanoparticles. *Small* **2022**, *19* (1), 2205474.

(13) Song, G. S.; Cheng, L.; Chao, Y.; Yang, K.; Liu, Z. Emerging Nanotechnology and Advanced Materials for Cancer Radiation Therapy. *Adv. Mater.* **2017**, *29* (32), 1700996.

(14) Hai, Z. J.; Ni, Y. H.; Saimi, D.; Yang, H. Y.; Tong, H. Y.; Zhong, K.; Liang, G. L. γ-Glutamyltranspeptidase-Triggered Intracellular Gadolinium Nanoparticle Formation Enhances the T_2-Weighted MR Contrast of Tumor. *Nano Lett.* **2019**, *19* (4), 2428−2433.

(15) Cai, Y.; Wang, Y. Q.; Xu, H. T.; Cao, C. Q.; Zhu, R. X.; Tang, X.; Zhang, T. W.; Pan, Y. X. Positive magnetic resonance angiography using ultrafine ferritin-based iron oxide nanoparticles. *Nanoscale* **2019**, *11* (6), 2644−2654.

(16) Seo, S.-J.; Chen, M. W.; Wang, H. X.; Kang, M. S.; Leong, K. W.; Kim, H.-W. Extra- and intra-cellular fate of nanocarriers under dynamic interactions with biology. *Nano Today* **2017**, *14*, 84−99.

(17) Zhang, Y. X.; Hai, Y.; Miao, Y. Q.; Qi, X.; Xue, W. M.; Luo, Y. E.; Fan, H. M.; Yue, T. L. The toxicity mechanism of different sized iron nanoparticles on human breast cancer (MCF7) cells. *Food Chem.* **2021**, *341* (Pt 2), 128263.

(18) Tang, Y. X.; Wang, X. Y.; Li, J.; Nie, Y.; Liao, G. J.; Yu, Y.; Li, C. Overcoming the Reticuloendothelial System Barrier to Drug Delivery with a "Don't-Eat-Us" Strategy. *ACS Nano* **2019**, *13* (11), 13015−13026.

(19) Tang, T.; Howarth, S. P.; Miller, S. R.; Trivedi, R.; Graves, M. J.; King-Im, J. U.; Li, Z. Y.; Brown, A. P.; Kirkpatrick, P. J.; Gaunt, M. E.; Gillard, J. H. Assessment of inflammatory burden contralateral to the symptomatic carotid stenosis using high-resolution ultrasmall, superparamagnetic iron oxide-enhanced MRI. *Stroke* **2006**, *37* (9), 2266−2270.

(20) Jiang, X. E.; Röcker, C.; Hafner, M.; Brandholt, S.; Dörlich, R. M.; Nienhaus, G. U. Endo- and exocytosis of zwitterionic quantum dot nanoparticles by live HeLa cells. *ACS Nano* **2010**, *4* (11), 6787−6797.

(21) Yanes, R. E.; Tarn, D.; Hwang, A. A.; Ferris, D. P.; Sherman, S. P.; Thomas, C. R.; Lu, J.; Pyle, A. D.; Zink, J. I.; Tamanoi, F. Involvement of lysosomal exocytosis in the excretion of mesoporous silica nanoparticles and enhancement of the drug delivery effect by exocytosis inhibition. *Small* **2013**, *9* (5), 697−704.

(22) Serda, R. E.; Mack, A.; van de Ven, A. L.; Ferrati, S.; Dunner, K., Jr.; Godin, B.; Chiappini, C.; Landry, M.; Brousseau, L.; Liu, X. W.; Bean, A. J.; Ferrari, M. Logic-embedded vectors for intracellular partitioning, endosomal escape, and exocytosis of nanoparticles. *Small* **2010**, *6* (23), 2691−2700.

(23) Ferrati, S.; McConnell, K. I.; Mack, A. C.; Sirisaengtaksin, N.; Diaz, R.; Bean, A. J.; Ferrari, M.; Serda, R. E. Cellular communication via nanoparticle-transporting biovesicles. *Nanomedicine (Lond)* **2014**, *9* (5), 581−592.

(24) Pandit, S.; Dutta, D.; Nie, S. Active transcytosis and new opportunities for cancer nanomedicine. *Nat. Mater.* **2020**, *19* (5), 478−480.

(25) Wen, X.; Ou, L.; Cutshaw, G.; Uthaman, S.; Ou, Y. C.; Zhu, T.; Szakas, S.; Carney, B.; Houghton, J.; Gundlach-Graham, A.; Rafat, M.; Yang, K.; Bardhan, R. Physicochemical Properties and Route of Systemic Delivery Control the In Vivo Dynamics and Breakdown of Radiolabeled Gold Nanostars. *Small* **2023**, *19* (29), 2204293.

(26) Gu, J. L.; Xu, H. F.; Han, Y. H.; Dai, W.; Hao, W.; Wang, C. Y.; Gu, N.; Xu, H. Y.; Cao, J. M. The internalization pathway, metabolic fate and biological effect of superparamagnetic iron oxide nanoparticles in the macrophage-like RAW264.7 cell. *Sci. China Life Sci. (2.297)* **2011**, *54* (9), 793−805.
(27) Shang, L.; Nienhaus, K.; Nienhaus, G. U. Engineered nanoparticles interacting with cells: size matters. *J. Nanobiotechnol.* **2014**, *12*, 5.
(28) Shang, L.; Xie, Q.; Yang, C.; Kong, L.; Zhang, Z. Extracellular Vesicles Facilitate the Transportation of Nanoparticles within and between Cells for Enhanced Tumor Therapy. *ACS Appl. Mater. Interfaces* **2023**, *15*, 42378−42394.
(29) El-Kenawi, A. With macrophages, tumors won't go hungry. *Sci. Transl. Med.* **2019**, *11* (487), No. eaax1722.
(30) Sakhtianchi, R.; Minchin, R. F.; Lee, K. B.; Alkilany, A. M.; Serpooshan, V.; Mahmoudi, M. Exocytosis of nanoparticles from cells: role in cellular retention and toxicity. *Adv. Colloid Interface Sci.* **2013**, *201*−*202*, 18−29.
(31) Zhang, H.; Li, L.; Liu, X. L.; Jiao, J.; Ng, C. T.; Yi, J. B.; Luo, Y. E.; Bay, B. H.; Zhao, L. Y.; Peng, M. L.; Gu, N.; Fan, H. M. Ultrasmall Ferrite Nanoparticles Synthesized via Dynamic Simultaneous Thermal Decomposition for High-Performance and Multifunctional T1Magnetic Resonance Imaging Contrast Agent. *ACS Nano* **2017**, *11* (4), 3614−3631.
(32) Chen, C. K.; Jones, C. H.; Mistriotis, P.; Yu, Y.; Ma, X. N.; Ravikrishnan, A.; Jiang, M.; Andreadis, S. T.; Pfeifer, B. A.; Cheng, C. Poly(ethylene glycol)-block-cationic polylactide nanocomplexes of differing charge density for gene delivery. *Biomaterials* **2013**, *34* (37), 9688−9699.
(33) Schmittgen, T. D.; Livak, K. J. Analyzing real-time PCR data by the comparative C(T) method. *Nat. Protoc.* **2008**, *3* (6), 1101−1108.
(34) Ankamwar, B.; Lai, T. C.; Huang, J. H.; Liu, R. S.; Hsiao, M.; Chen, C. H.; Hwu, Y. K. Biocompatibility of Fe(3)O(4) nanoparticles evaluated by in vitro cytotoxicity assays using normal, glia and breast cancer cells. *Nanotechnology* **2010**, *21* (7), 075102.
(35) Lai, S.; Centi, S.; Borri, C.; Ratto, F.; Cavigli, L.; Micheletti, F.; Kemper, B.; Ketelhut, S.; Kozyreva, T.; Gonnelli, L.; Rossi, F.; Colagrande, S.; Pini, R. A multifunctional organosilica cross-linker for the bio-conjugation of gold nanorods. *Colloids Surf. B Biointerfaces* **2017**, *157*, 174−181.
(36) Canton, I.; Battaglia, G. Endocytosis at the nanoscale. *Chem. Soc. Rev.* **2012**, *41* (7), 2718−2739.
(37) Debnath, K.; Pal, S.; Jana, N. R. Chemically Designed Nanoscale Materials for Controlling Cellular Processes. *Acc. Chem. Res.* **2021**, *54* (14), 2916−2927.
(38) Erlichman, J. S.; Leiter, J. C. Complexity of the Nano-Bio Interface and the Tortuous Path of Metal Oxides in Biological Systems. *Antioxidants* **2021**, *10* (4), 547.
(39) García, I.; Henriksen-Lacey, M.; Calvo, J.; de Aberasturi, D. J.; Paz, M. M.; Liz-Marzán, L. M. Size-Dependent Transport and Cytotoxicity of Mitomycin-Gold Nanoparticle Conjugates in 2D and 3D Mammalian Cell Models. *Bioconjugate Chem.* **2019**, *30* (1), 242−252.
(40) Liu, J.; Liu, Y.-Y.; Li, C.-S.; Cao, A.; Wang, H. Exocytosis of Nanoparticles: A Comprehensive Review. *Nanomaterials-Basel* **2023**, *13* (15), 2215.
(41) Lai, S. K.; Hida, K.; Man, S. T.; Chen, C.; Machamer, C.; Schroer, T. A.; Hanes, J. Privileged delivery of polymer nanoparticles to the perinuclear region of live cells via a non-clathrin, non-degradative pathway. *Biomaterials* **2007**, *28* (18), 2876−2884.
(42) Tang, P. S.; Sathiamoorthy, S.; Lustig, L. C.; Ponzielli, R.; Inamoto, I.; Penn, L. Z.; Shin, J. A.; Chan, W. C. W. The Role of Ligand Density and Size in Mediating Quantum Dot Nuclear Transport. *Small* **2014**, *10* (20), 4182−4192.
(43) Liu, M. M.; Li, Q.; Liang, L.; Li, J.; Wang, K.; Li, J. J.; Lv, M.; Chen, N.; Song, H. Y.; Lee, J.; Shi, J. Y.; Wang, L. H.; Lal, R.; Fan, C. H. Real-time visualization of clustering and intracellular transport of gold nanoparticles by correlative imaging. *Nat. Commun.* **2017**, *8*, 15646.
(44) Zhang, X. D.; Liang, X.; Gu, J. J.; Chang, D. F.; Zhang, J. X.; Chen, Z. W.; Ye, Y. Q.; Wang, C.; Tao, W.; Zeng, X. W.; Liu, G.; Zhang, Y. J.; Mei, L.; Gu, Z. Investigation and intervention of autophagy to guide cancer treatment with nanogels. *Nanoscale* **2017**, *9* (1), 150−163.
(45) Hutagalung, A. H.; Novick, P. J. Role of Rab GTPases in membrane traffic and cell physiology. *Physiol Rev.* **2011**, *91* (1), 119−149.
(46) Pfeffer, S. R. Rab GTPase regulation of membrane identity. *Curr. Opin. Cell Biol.* **2013**, *25* (4), 414−419.
(47) Stenmark, H. Rab GTPases as coordinators of vesicle traffic. *Nat. Rev. Mol. Cell Biol.* **2009**, *10* (8), 513−525.
(48) Zhu, X. B.; Ji, X. Y.; Kong, N.; Chen, Y. H.; Mahmoudi, M.; Xu, X. D.; Ding, L.; Tao, W.; Cai, T.; Li, Y. J.; Gan, T.; Barrett, A.; Bharwani, Z.; Chen, H. B.; Farokhzad, O. C. Intracellular Mechanistic Understanding of 2D MoS(2) Nanosheets for Anti-Exocytosis-Enhanced Synergistic Cancer Therapy. *ACS Nano* **2018**, *12* (3), 2922−2938.
(49) Wandinger-Ness, A.; Zerial, M. Rab proteins and the compartmentalization of the endosomal system. *Cold Spring Harb Perspect Biol.* **2014**, *6* (11), a022616.
(50) Zhang, J. X.; Zhang, X. D.; Liu, G.; Chang, D. F.; Liang, X.; Zhu, X. B.; Tao, W.; Mei, L. Intracellular Trafficking Network of Protein Nanocapsules: Endocytosis, Exocytosis and Autophagy. *Theranostics* **2016**, *6* (12), 2099−2113.
(51) Ding, L.; Zhu, X. B.; Wang, Y. L.; Shi, B. Y.; Ling, X.; Chen, H. J.; Nan, W. H.; Barrett, A.; Guo, Z. L.; Tao, W.; Wu, J.; Shi, X. J. Intracellular Fate of Nanoparticles with Polydopamine Surface Engineering and a Novel Strategy for Exocytosis-Inhibiting, Lysosome Impairment-Based Cancer Therapy. *Nano Lett.* **2017**, *17* (11), 6790−6801.
(52) Yang, Z. F.; Klionsky, D. J. Eaten alive: a history of macroautophagy. *Nat. Cell Biol.* **2010**, *12* (9), 814−822.
(53) Qiu, C.; Han, H. H.; Sun, J.; Zhang, H. T.; Wei, W.; Cui, S. H.; Chen, X.; Wang, J. C.; Zhang, Q. Regulating intracellular fate of siRNA by endoplasmic reticulum membrane-decorated hybrid nanoplexes. *Nat. Commun.* **2019**, *10* (1), 2702.
(54) Linford, A.; Yoshimura, S.; Bastos, R.; Langemeyer, L.; Gerondopoulos, A.; Rigden, D. J.; Barr, F. A. Rab14 and its exchange factor FAM116 link endocytic recycling and adherens junction stability in migrating cells. *Dev. Cell* **2012**, *22* (5), 952−966.
(55) Ding, L.; Yao, C.; Yin, X.; Li, C.; Huang, Y.; Wu, M.; Wang, B.; Guo, X.; Wang, Y.; Wu, M. Size, Shape, and Protein Corona Determine Cellular Uptake and Removal Mechanisms of Gold Nanoparticles. *Small* **2018**, *14*, No. e1801451.
(56) Zhang, J.; Qin, M.; Yang, D.; Yuan, L.; Zou, X.; Dai, W.; Zhang, H.; Wang, X.; He, B.; Zhang, Q. Nanoprotein Interaction Atlas Reveals the Transport Pathway of Gold Nanoparticles across Epithelium and Its Association with Wnt/β-Catenin Signaling. *ACS Nano* **2021**, *15* (11), 17977−17997.
(57) Liu, Y.; Huo, Y. Y.; Yao, L.; Xu, Y. W.; Meng, F. Q.; Li, H. F.; Sun, K.; Zhou, G. D.; Kohane, D. S.; Tao, K. Transcytosis of Nanomedicine for Tumor Penetration. *Nano Lett.* **2019**, *19* (11), 8010−8020.
(58) Fichter, K. M.; Ingle, N. P.; McLendon, P. M.; Reineke, T. M. Polymeric nucleic acid vehicles exploit active interorganelle trafficking mechanisms. *ACS Nano* **2013**, *7* (1), 347−364.
(59) Ross, N. L.; Munsell, E. V.; Sabanayagam, C.; Sullivan, M. O. Histone-targeted Polyplexes Avoid Endosomal Escape and Enter the Nucleus During Postmitotic Redistribution of ER Membranes. *Mol. Ther. Nucleic Acids* **2015**, *4* (2), No. e226.
(60) Feng, Y.; Yu, S.; Lasell, T. K.; Jadhav, A. P.; Macia, E.; Chardin, P.; Melancon, P.; Roth, M.; Mitchison, T.; Kirchhausen, T. Exo1: a new chemical inhibitor of the exocytic pathway. *Proc. Natl. Acad. Sci. U.S.A.* **2003**, *100* (11), 6469−6474.
(61) Maxfield, F. R.; McGraw, T. E. Endocytic recycling. *Nat. Rev. Mol. Cell Biol.* **2004**, *5* (2), 121−132.
(62) Sikora, B.; Kowalik, P.; Mikulski, J.; Fronc, K.; Kamińska, I.; Szewczyk, M.; Konopka, A.; Zajdel, K.; Minikayev, R.; Sobczak, K.;

https://doi.org/10.1021/acsomega.3c07081
ACS Omega 2024, 9, 3480−3490

Zaleszczyk, W.; Borodziuk, A.; Rybusiński, J.; Szczytko, J.; Sienkiewicz, A.; Wojciechowski, T.; Stępień, P.; Frontczak-Baniewicz, M.; Łapiński, M.; Wilczyński, G.; Paszkowicz, W.; Twardowski, A.; Elbaum, D. Mammalian cell defence mechanisms against the cytotoxicity of NaYF(4):(Er,Yb,Gd) nanoparticles. *Nanoscale* **2017**, *9* (37), 14259−14271.

https://doi.org/10.1021/acsomega.3c07081
ACS Omega 2024, 9, 3480−3490